Biomicrofluidics ARTICLE scitation.org/journal/bmf

Dual shape recovery of red blood cells flowing out of a microfluidic constriction

Cite as: Biomicrofluidics 14, 024116 (2020); doi: 10.1063/5.0005198
Submitted: 19 February 2020 · Accepted: 1 April 2020 ·
Published Online: 28 April 2020

View Online Export Citation CrossMark

A. Amirouche,[1] J. Esteves,[1] A. Lavoignat,[2] S. Picot,[2,3] R. Ferrigno,[1] and M. Faivre[1,a)]

AFFILIATIONS

[1]Université de Lyon, Institut des Nanotechnologies de Lyon INL-UMR5270 CNRS, Université Lyon 1, Villeurbanne F-69622, France
[2]Malaria Research Unit, SMITh, Institut de Chimie et de Biochimie Moléculaires et Supramoléculaires ICBMS-UMR5246 CNRS, Université Lyon 1, Villeurbanne F-69622, France
[3]Institute of Parasitology and Medical Mycology, Croix-Rousse Hospital, Hospices Civils de Lyon, 69004 Lyon, France

[a)]**Author to whom correspondence should be addressed:** magalie.faivre@univ-lyon1.fr

ABSTRACT

Micropipette aspiration, optical tweezers, rheometry, or ecktacytometry have been used to study the shape recovery of healthy human Red Blood Cells (RBCs) and measure associated relaxation times of the order of 100–300 ms. These measurements are in good agreement with the Kelvin–Voigt model, which describes the cell as a visco-elastic material, predicting that its relaxation time only depends on cell intrinsic properties. However, such mechanical solicitation techniques are far from being relevant regarding RBC solicitation *in vivo*. In this paper, we report for the first time the existence of two different behaviors of the RBC shape recovery while flowing out of a microfluidic constricted channel. The calculation of the viscous stress corresponding to the frontier between the two recovery modes confirms that the RBC resistance to shear μ is the elastic property dominating the transition between the two recovery behaviors. We also quantified associated recovery times τ_r and report values as low as 4 ms—which is almost two decades smaller than the typical RBC relaxation time—at high viscosity and flow velocity of the carrier fluid. Although we cannot talk about relaxation time because the cell is never at rest, we believe that the measured shape recovery time arises from the coupling of the cell intrinsic deformability and the hydrodynamic stress. Depending on the flow conditions, the cell mechanics becomes dominant and drives the shape recovery process, allowing the measurement of recovery times of the same order of magnitude than relaxation times previously published. Finally, we demonstrated that the measurement of the shape recovery time can be used to distinguish *Plasmodium falciparum* (causing malaria) infected RBCs from healthy RBCs.

I. INTRODUCTION

The Red Blood Cell (RBC) membrane is composed of a phospholipidic bilayer, associated with a 2D spectrin network composing the cytoskeleton[1] and enclosing a viscous cytoplasm loaded with hemoglobin. The mechanical properties of the cytoskeleton combined with a high surface to volume ratio give RBCs an impressive ability for reversible deformation. This particular property is very crucial for RBCs as they spend their 120 days of life flowing through microcapillaries to transport oxygen through the whole organism. The combination between the phospholipid bilayer and the cytoskeleton constituting its membrane confers to the RBC a visocoelastic behavior, which is intermediary between that of an elastic solid, characterized by energy conservation and a purely viscous Newtonian liquid, characterized by energy dissipation. This type of behavior can be described by the Kelvin–Voigt model,[2] which is a linear combination of a spring and a damping Newtonian element. Using the Kelvin–Voigt model, the pioneering study of Hochmuth *et al.*[3] predicted that the time necessary for RBCs to relax, from a deformed state to their stress-free equilibrium shape, is a constant, which depends only on the mechanical properties of the membrane. This constant is defined as $\tau = \eta_m/\mu$, where η_m is the 2D membrane viscosity and μ, its shear modulus.

Knowing that η_m has been estimated[4–6] to be of the order of magnitude of $0.5–1 \times 10^{-6}$ N s/m and that μ has been measured experimentally through different methods[3,4,7–10] in the range $\mu = 2.5–9 \times 10^{-6}$ N/m, τ can be calculated to be of the order of 100 ms.

Different methods have been reported in the literature to characterize experimentally this relaxation time τ in static

configurations, such as micropipette aspiration,[8,11,12] optical tweezers,[3,13] and electrodeformation.[14] τ has also been measured under flow conditions, as, for example, using rheometry,[15,16] ecktacytometry,[17] and more recently microfluidics.[18] All of these studies, which have been performed in low viscosity physiological buffer as the external medium, either in static or under flow, report roughly the same relaxation time to be of the order of 100–300 ms.[8,11,15,18] Those values are in good agreement with the calculation of τ made by Hochmuth using the Kelvin–Voigt model to describe the RBC mechanics.

In the present paper, we propose to study experimentally the shape recovery of healthy human RBCs flowing out of a microfluidic constricted channel. We report for the first time two different types of shape recovery behaviors for the cell after exiting the constricted channel, depending on the viscous stress applied. We demonstrated that the transition between the two recovery modes is directly related to the RBC elastic properties. We measured experimentally associated shape recovery times, τ_r, defined as the time necessary for the cell to return to a steady shape after exiting the constricted geometry. Because RBC steady state is reached under hydrodynamic stress rather than at rest, the recovery time does not directly correspond to the relaxation time. However, in specific experimental conditions, values obtained for recovery times were found to be comparable to typical intrinsic relaxation time values reported in the literature while reaching values as low as 4 ms with very different flow parameters. From the highly abundant literature dealing with the flow of RBCs in close-fitting constriction, only the paper from Braunmüller *et al.*[18] looked at the RBC shape relaxation. They report the existence of two relaxation times. A first relaxation time τ_1, corresponding to the time necessary to change from the compressed shape inside the microchannel to adopt the parachute-like shape, is found to be in the range 0.11–0.52 s, which is in good agreement with relaxation times reported by others. The second time, $\tau_{1/2}$, corresponds to the time necessary to deform from the parachute-like shape to the discoidal shape and was measured to be of the order of 9–49 s. They found that the two times vary linearly with respect to each other. However, to the best of our knowledge, we are the first ones highlighting the coupling between the cell mechanics and the hydrodynamics at the exit of a microfluidic constriction, by measuring the variation of shape recovery time upon buffer viscosity and flow speed. Finally, the use of the shape recovery time to discriminate healthy from pathological cells was demonstrated on *Plasmodium falciparum* infected RBCs (iRBCs).

II. MATERIALS AND METHODS

A. Experiments

1. Device geometry

The microfluidic systems were made in polydimethylsiloxane (PDMS, Sylgard), using standard soft-lithography techniques[19] and sealed on glass *via* an oxygen plasma treatment (Harrick plasma). The main width of the channel W_o was set to 15, 25 and 50 μm while keeping a fixed height of 5 μm. A succession of 15 tooth-like shapes—composed of a narrowing followed by a widening—were implemented. This geometry is referred to as the oscillating width channel (OWC). In the zone of interest of the geometry, the channel width decreases from W_o to 5 μm and then increases up to 25 μm. Each constriction and widening has a length of 10 μm, and this width oscillation is repeated over a total length $L = 290\,\mu$m as illustrated in Fig. 1. This specific geometry was chosen for its ability to quickly center RBCs (cf. Fig. 2).

2. Suspension preparation

30 μl of fresh blood were drawn from healthy volunteers by finger prick. RBCs were isolated from the rest of the sample by centrifugation and then re-suspended in phosphate buffered saline (PBS, Sigma-Aldrich, France), in which viscosity η_{out} was varied from 1.3 to 31.5 mPa s, by solubilization of Dextran (Leuconostoc mesenteroides, $M_w = 2 \times 10^6$, Sigma-Aldrich, France). All solutions were filtered at 200 nm prior to utilization. The RBC concentration was adjusted to approximately 19×10^6 RBCs/ml in order to avoid the flow of several cells simultaneously in the microchannel. Malaria infected RBCs (iRBCs) were obtained by culture of 3D7 *Plasmodium falciparum* clone maintained *in vitro* as previously described.[20] Healthy human RBCs were suspended in Roswell Park Memorial Institute Medium (RPMI) culture medium supplemented with 0.5% AlbuMAX^{TM} II, 2.1 g l^{-1} $NaHCO_3$, 0.025 g l^{-1} Hypoxanthine, 25 mM HEPES, and 20 μg ml^{-1} Gentamicin at 5% hematocrit and inoculated with infected RBCs. Enrichment of iRBCs was obtained using a Percoll discontinuous density gradient centrifugation method.[21] The isolated iRBC layer was washed three times in the culture medium before being suspended in supplemented RPMI. Parasitemia was evaluated by microscopical examination of Giemsa colored blood smear at roughly 80% as illustrated in Fig. 1 in the supplementary material. Finally, iRBCs were washed twice with PBS and suspended in a viscous saline buffer ($\eta_{out} = 31.5$ mPa s) at the optimum concentration for microfluidic

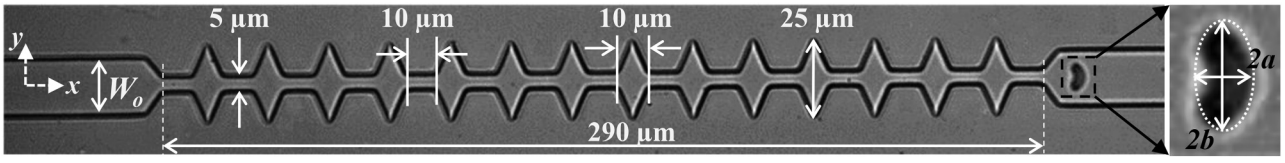

FIG. 1. The microfluidic channel used to study the shape recovery time of RBCs under confined flow is composed of 14 tooth-like shaped constrictions. The different dimensions are reported in the picture; here, $W_o = 15\,\mu$m. The inset shows a close-up of a RBC in which the 2D projected area is fitted by an ellipse (white dashed line). The two axes of the ellipse along and normal to the flow direction, respectively, 2*a* and 2*b*, are defined.

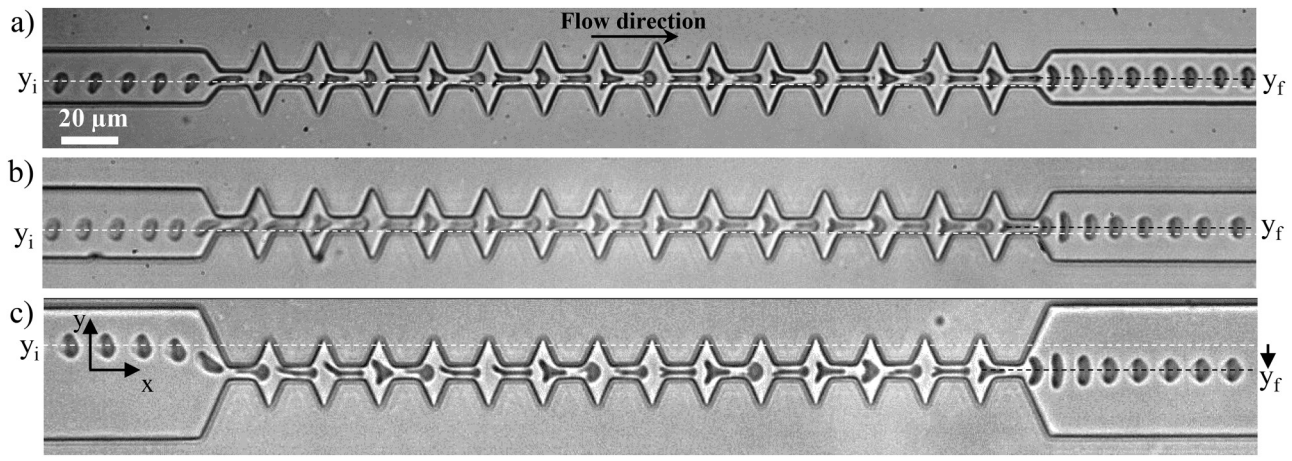

FIG. 2. Time lapse microscopic images of cells entering the microfluidic channel at various off-centered positions, denoted as y_i, and exiting centered in the channel, $y_f = 0$. The origin of the y axis was chosen to coincide with the center axis of the channel. (a) $W_o = 15\,\mu$m ($\eta_{out} = 31.5$ mPa s and $V_{cell} = 1820\,\mu$m s^{-1}), (b) $W_o = 25\,\mu$m ($\eta_{out} = 31.5$ mPa s and $V_{cell} = 2194\,\mu$m s^{-1}), and (c) $W_o = 50\,\mu$m ($\eta_{out} = 31.5$ mPa s and $V_{cell} = 1979\,\mu$m s^{-1}).

experiments. A more detailed version of the iRBC enrichment procedure can be found in the supplementary material.

3. Experimental setup

The RBC suspension was injected into the microfluidic channel using a pressure driven flow. The applied pressure was varied between 13 and 500 mbar depending on the targeted cell velocity. The lower pressure gradients were achieved using hydrostatic setup, i.e., a height difference was set between the syringe containing the blood sample and the outlet reservoir, whereas higher pressure gradients were applied using a pressure regulator (Bellofram and Fluigent) with a precision of 1 mbar. Video-microscopic recordings of the cells behavior were performed with an inverted phase contrast microscope (Leica DMI 4000 B, Germany) with a ×40 magnification and a high speed camera (Mikrotron EoSens MC1362, Germany).

4. Image analysis routine

Post-processing of the movies was performed using a self-edited Matlab code to study cell dynamics and deformation. On every image, the RBC contour was fitted with an elliptical shape (Fig. 1); the position of the ellipse center of mass and the length of both axes, along (x-direction) and perpendicular to (y-direction) the flow direction, respectively, $2a$ and $2b$, were measured. Various parameters were then calculated: the cells velocity V_{cell} (see Fig. 2 in the supplementary material for a detailed definition of V_{cell}) and the deformation index D, defined as $D = (2a - 2b)/(2a + 2b)$.

B. Numerical simulations

For the estimation of the hydrodynamic stress, 3D numerical simulations were performed using Comsol Multiphysics® to solve the hydrodynamic flow equations. Simulations were performed by applying a pressure gradient flow between the inlet and outlet of the microfluidic channel, using different values of fluid viscosities $\eta_{out} = 2.8$, 8.6, and 31.5 mPa s.

III. RESULTS AND DISCUSSIONS

A. Centering effect of the geometry

Although we focused in this paper on the cell behavior at the exit of a constricted channel, we have chosen to implement an oscillating width channel, including several 10 μm long constrictions, instead of a single 10 μm long one, because of the centering effect associated with the repetition of the restrictions. Indeed, one may notice from Fig. 2 that whatever their position in the inlet main microchannel, y_i, RBCs tended to exit the geometry at the same position y_f, associated with the half of W_o, hence illustrating the centering effect of the design. Several studies reported in the literature have used different techniques to focus cells and facilitate single cell study. For example, sheath flow, where two streams of liquid force the alignment of the cells on the chip, has been reported.[22] Similar results can be achieved using active approaches such as acoustophoresis[23] or electrophoresis.[24,25] The implementation of a geometrical constriction has been demonstrated to focus cells toward the centerline of the device when the width of the channel is subsequently increased.[26,27] Finally, in order to obtain a single file of cells, Tsai *et al.* have used a 4.5 μm wide and 30 μm long geometrical restriction to center RBCs and align them so they would enter the evaluation zone on the same streamline.[28]

In the case of a unique 10 μm long constriction, cells arriving off-centered in the channel tended to exit also off-centered. The centering effect associated with the oscillating width channel ensures a symmetrical deformation of the cells at the exit of the last narrowing, prevents them from rotating, and imposes that all cells are exposed to the same hydrodynamic stress, all cells being aligned on the same flow line. This centering effect is more pronounced for

W_o = 50 μm, where it is more necessary as cells might arrive from various off-centered positions. Indeed, we can see that the centering amplitude $|y_i - y_f|$, illustrated by the dashed lines, is larger for $W_o = 50\,\mu$m (see Fig. 3 in the supplementary material). Finally, we have verified that the history of deformation, via the repetition of the constrictions, did not impact the mechanical response of healthy RBC (hRBC), by measuring the recovery time of healthy RBCs both after one single 10 μm long geometric restriction and at the exit of the 15 repetitions of the 10 μm long restriction (see Fig. 4 in supplementary material).

B. Dual shape recovery behavior

Video-microscopic recordings of RBCs flowing through a microfluidic channel with oscillating width allowed the visualization of cell deformation as it traveled through the device. The cell entering the 15 μm wide channel presented a parachute-like shape, typical of RBCs in confined flow. As it approached the first constriction, the cell got compressed, which is traduced by its elongation in the flow direction (Fig. 2).

Then, it underwent a stretching along the y-axis when entering the widening, before being compressed again by the next constriction. This cycle of compression-stretching is repeated due to the series of narrowings and enlargements. Finally, as it exited the last narrowing, the cell returns to its final parachute-like shape. Because the steady state does not correspond to resting conditions, the recovery process by which cells return to their final shape, after flowing out of the geometry, cannot be directly assimilated to a cell relaxation. Thus, this recovery process does not depend only on its mechanics but rather on a coupling between the relaxation and the flow. At the exit, two different recovery behaviors were observed according to the experimental conditions as illustrated by the sequences of the deformation presented in Fig. 3.

At high speed and viscosity of the carrier fluid [Fig. 3(a)], we observed a first recovery mode—the stretching behavior—which is characterized by a sudden increase of the $2b$-axis (normal to the flow direction) of the cell as it exited the last constriction, before recovering slowly its steady state shape as illustrated on the schematic and highlighted on the time lapse close-up [Fig. 3(a)]. At lower speed and external viscosity [Fig. 3(b)], the cell underwent the same compression-stretching cycles and behaved qualitatively similarly with a lower amplitude of deformation than the previous mode in the central zone of the microchannel. However, at the exit, the cell, which was compressed due to the last narrowing, recovers directly a

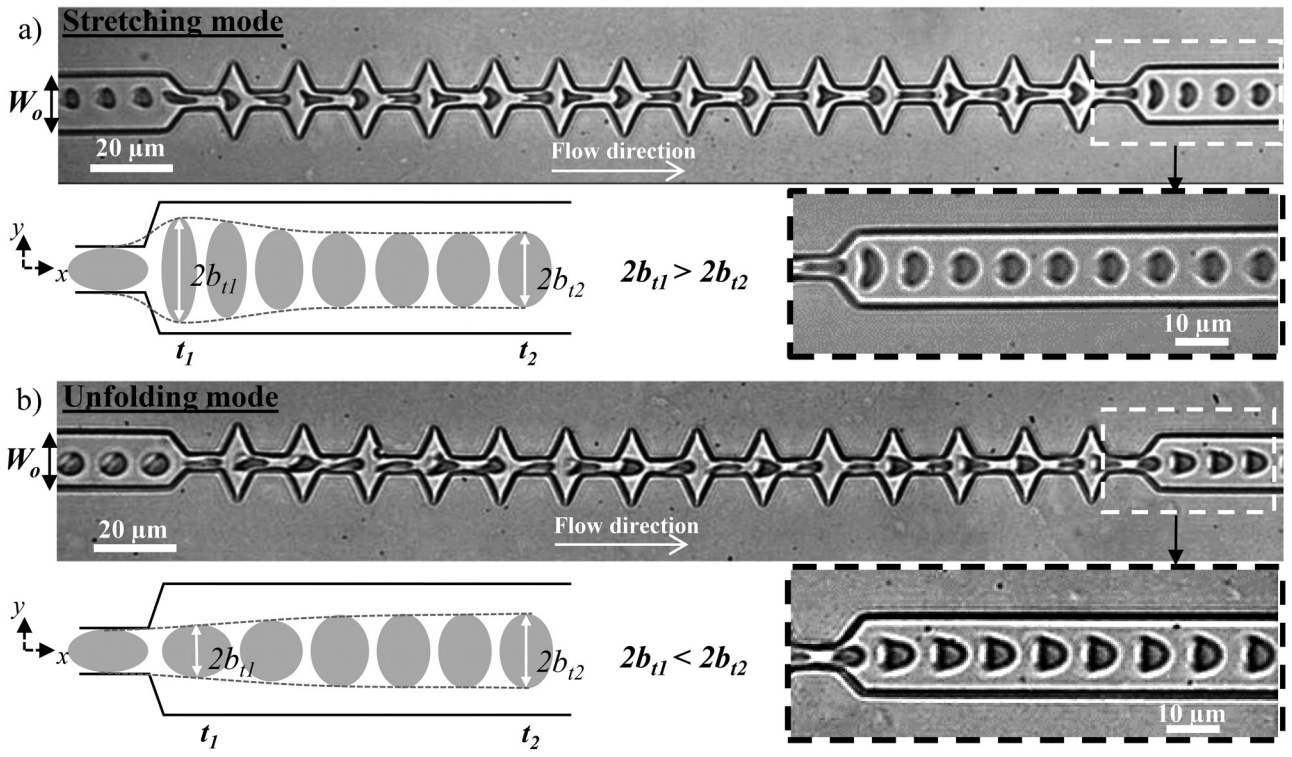

FIG. 3. Sequences of the deformation of two healthy RBCs under flow (a) at high and (b) at low speed and viscosity of the external medium. Along the geometry, both cells get compressed and elongated perpendicular to the flow direction when entering each narrowing and widening, respectively. (a) At high hydrodynamic stress, as the cell exits, it is stretched by the extensional flow before returning to the parachute-like shape, unlike at lower stress (b), where the cell recovers directly from the compression without being stretched. The external viscosity and the cell speed at the exit are, respectively, (a) $\eta_{out} = 31.5$ mPa s and $V_{cell} = 533\,\mu$m s^{-1} and (b) $\eta_{out} = 1.3$ mPa s and $V_{cell} = 483\,\mu$m s^{-1}. The schematics show a representation of the typical deformation in the two behaviors at two different times t_1 and t_2.

parachute-like shape, without being stretched in the y-direction as pointed out on the schematic and the time lapse close-up [Fig. 3(b)]. This mode is referred to as the unfolding behavior.

The deformation of the RBCs flowing in our geometry can be quantified using the deformation index $D = (2a - 2b)/(2a + 2b)$, where $2a$ and $2b$ are the two axes of the elliptical shape fitting the cell. As an example, the variation of D associated with the sequences of deformation presented in Fig. 3 is reported in Fig. 4.

As the RBC maintained its parachute-like shape, in the 15 μm wide zone of the channel, the corresponding deformation index was relatively constant and nearly close to zero, hence traducing a projected area roughly circular ($2a = 2b$). The following oscillations in D traduced the deformation undergone by the RBC in response to the oscillating width of the channel. Indeed, D increased to positive values ($2a > 2b$) due to the cell compression by the constriction [Figs. 4(a) and 4(c) upper photo] leading to its elongation in the flow direction. On the contrary, when entering an enlargement, it tended to be stretched in the y-direction [Figs. 4(a) and 4(c), lower photo] corresponding to a decrease in D, which can reach negative values ($2a < 2b$) depending on the experimental conditions.

In the stretching behavior [Fig. 4(a)], after reaching a maximum value at $x = 285\,\mu$m, the sudden drop of D traduces the large cell stretching after its exit from the last narrowing. Finally, after reaching a minimum, noted D_{out}, around $x = 295\,\mu$m, D returns exponentially to its initial value and reaches a plateau corresponding to the cell steady shape. In the case of the unfolding behavior presented in Fig. 4(c), D reaches a maximum value at $x = 285\,\mu$m, denoted as D_{out}; however, it recovers directly a steady shape according to an exponential decay.

The variation of D between the last deformed state at the exit, noted D_{out}, and the steady shape corresponding to the plateau value were represented as a function of time [Figs. 4(b) and 4(d)]. The experimental data were fitted using an exponential growth or decay, depending on the stretching or unfolding mode, respectively, thus allowing the extraction of the recovery time τ_r.

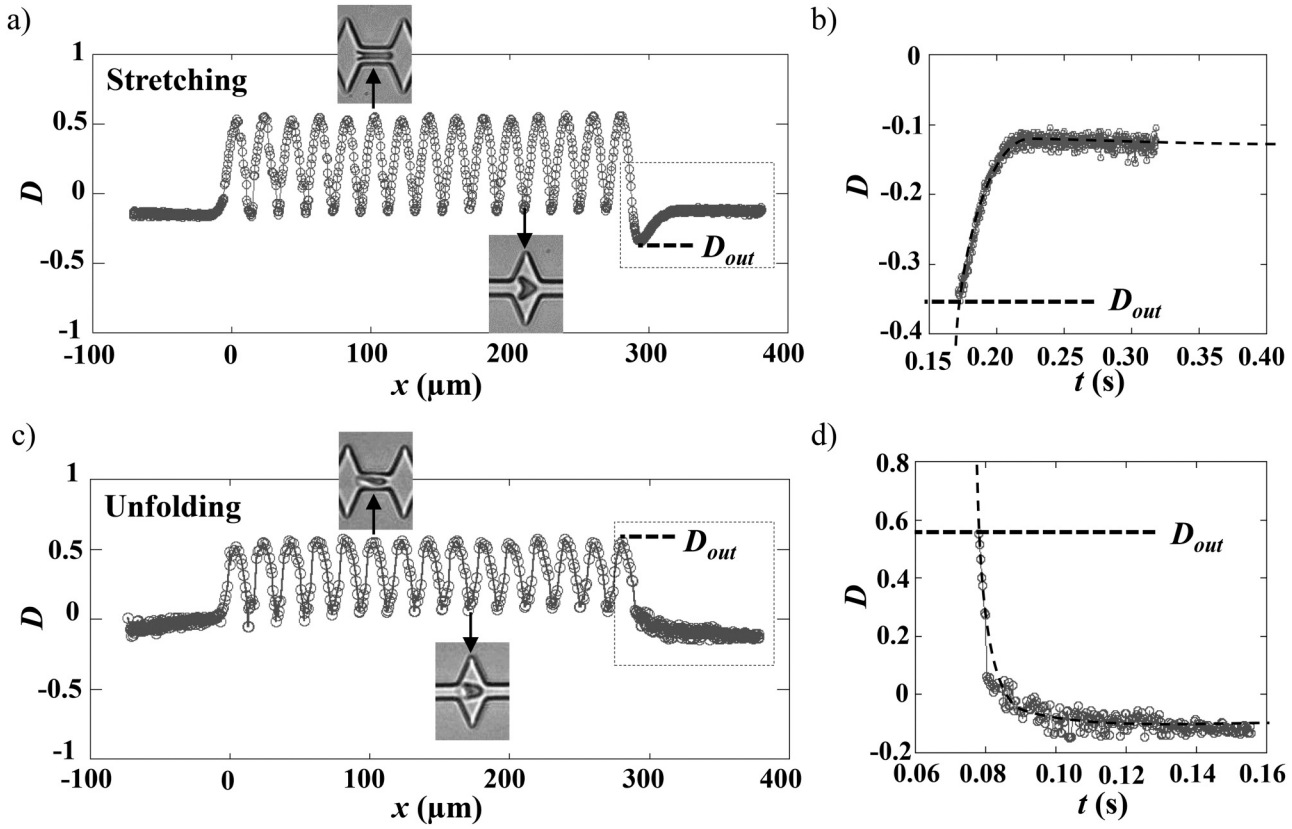

FIG. 4. Variation of the deformation index $D = (2a - 2b)/(2a + 2b)$ vs the position of the cell center of mass (a) and (b) for the stretching and (c) and (d) for the unfolding behaviors. The origin of the graphs was arbitrarily chosen to be the entry of the first narrowing. (b) and (d) show representations of D vs time of the two previous curves, where only the time window corresponding to the recovery is reported. The exit of the last narrowing was arbitrarily chosen to be $t = 0$. The dashed lines are exponential fits allowing the determination of the recovery time τ_r, with the following equations $D = m_1 + m_2 \exp((m_3 - t)/\tau_r)$ and $D = m_1 + m_2 \exp(-(m_3 + t)/\tau_r)$, for unfolding and stretching, respectively, where m_1, m_2, and m_3 are constants to be adjusted.

C. The transition between the two recovery behaviors depends on RBC elastic properties

We evaluated the influence of external flow parameters on the shape recovery of healthy RBCs by varying buffer viscosities and cell velocities. We scanned a range of cell speeds from 100 to 2000 μm s^{-1} and the external viscosity was varied from 1 to 31.5 mPa s. We gathered experimental results in a diagram (Fig. 5), where the recovery mode is plotted as a function of η_{out} and V_{cell}.

For $V_{cell} \geq 400\,\mu$m s^{-1}, stretching was observed experimentally for $\eta_{out} \geq 5$ mPa s, whereas unfolding was obtained for $\eta_{out} \leq 2$ mPa s. Thus, in this range of cell speed, the transition between the two recovery modes is mainly dictated by η_{out}. In the frontier zone (highlighted by the dashed line in Fig. 5), we noticed experimentally a mixed behavior, where a portion of the RBC population experienced stretching, while the other one experienced unfolding. The percentage of the stretching behavior increased with the cell velocity, hence highlighting that the transition depends also on V_{cell}. At a lower cell speed, $V_{cell} \leq 350\,\mu$m s^{-1}, the transition between the two recovery modes depended strongly on both V_{cell} and η_{out}.

By increasing the viscosity and velocity of the carrier fluid, we tuned the viscous hydrodynamic stress probed by RBCs, which leads to a transition in shape recovery behavior. Indeed, the diagram reveals that at low viscous stress, the cell resists the deformation and recovers a steady shape according to the unfolding mode, whereas, when the viscous stress is sufficiently high, the RBC gets stretched at the exit and experiences stretching. Therefore, the Capillary number, ratio of the fluid viscous forces to the RBC elastic properties, can be used to describe the shape recovery of RBCs. To elucidate which elastic property dictates the experimental shape recovery of healthy RBCs, we aim at calculating the three Capillary numbers $Ca_{bending} = \frac{St.(2b)^3}{B}$, $Ca_{shear} = \frac{St.2b}{\mu}$, and $Ca_{stretching} = \frac{St.2b}{K}$, associated with the bending modulus B, the shear modulus μ and the stretching modulus K, respectively, $2b$ being the typical size of cells. In parallel, the viscous stress St undergone by RBCs at the exit of our geometry was estimated using relation [Eq. (1)]. In a diverging channel, St can be expressed[29] as

$$St \sim 3\eta_{out}\left[\left|\frac{\partial u}{\partial x}\right| + \left|\frac{\partial v}{\partial y}\right|\right]. \quad (1)$$

In order to estimate St probed by the cell at the exit, we used Comsol Multiphysics® to perform 3D simulations of the flow of buffer solutions at various viscosities in absence of any object. We calculated the local stress St, according to Eq. (1) [see Fig. 5 in the supplementary material], for various conditions of η_{out} and V_{Fluid}, with V_{Fluid} corresponding to the maximum velocity of the parabolic profile at the exit of the last constriction. In a first approximation, we considered the velocity gradients at the exit of the oscillating width channel in absence of cells.

As expected, Fig. 6 illustrates that St increases linearly with V_{Fluid} and varies also with η_{out}. We report on the graph, the domains where each of the recovery modes is observed experimentally, assuming in a first approximation that $V_{Fluid} \sim V_{cell}$. From Fig. 6, we could estimate a range of local stress, St_{thresh}, corresponding to the frontier between the two modes.

For hydrodynamic stresses larger than St_{thresh}, RBCs are deformed and underwent a stretching behavior, whereas for lower stresses, they experienced unfolding. For $\eta_{out} = 2.8$ mPa s and V_{Fluid} ranging from 460 to 1018 μm s^{-1}, the zone of the relaxation diagram where the mixed behavior was observed, we estimated St_{thresh} to be between 0.6 and 1.4 Pa.

Using this threshold stress and reading the graph in Fig. 6, we can estimate that unfolding behavior would be observed for V_{cell} below 140 μm s^{-1} and 25 μm s^{-1}, for $\eta_{out} = 8.6$ mPa s and 31.5 mPa s, respectively. This was consistent with our experimental observations for these two viscosity values. Indeed, minimum velocities that we could reach experimentally were $V_{cell} = 277\,\mu$m s^{-1} for $\eta_{out} = 8.6$ mPa s, and $V_{cell} = 133\,\mu$m s^{-1} for $\eta_{out} = 31.5$ mPa s, values above the extrapolated frontier values found previously. Therefore, we only observed stretching for these buffer viscosities.

RBC elastic moduli have been previously reported in the literature[2,30–32] to be $B = 1.8 \times 10^{-19}$ N m, $\mu = 2.5$–$9\,\mu$N m^{-1}, and $K = 2 \times 10^5\,\mu$N m^{-1}. These values allow the calculation of the associated Capillary numbers to be of the order of $Ca_{bending} \sim 10^3$, $Ca_{shear} \sim 1$, and $Ca_{stretching} \sim 10^{-5}$, respectively. Therefore, we can conclude that the shear modulus drives the transition between the recovery behaviors of RBCs. It would be interesting to try to determine if the study of RBC shape recovery at the exit of a microfluidic constriction could be a novel way to evaluate RBC elastic shear modulus, although experiments performed with mechanically altered RBCs are required in order to demonstrate it. Mechanically altered RBCs would have to be flown at several speed in our geometry, while being suspended in buffers with various viscosities in order to determine the associated threshold stress St_{thresh}. But more importantly, a quantitative measurement of the Young modulus of the impaired RBCs would be necessary to validate our hypothesis.

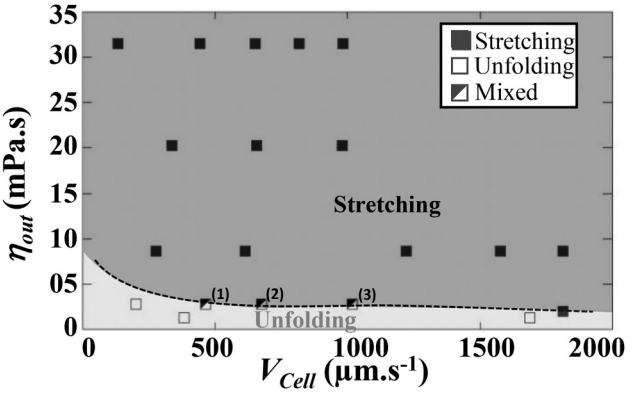

FIG. 5. Experimental recovery diagram representing unfolding (open squares) or stretching (solid squares) behaviors according to the cell velocity V_{cell} and the viscosity of the surrounding medium η_{out}. The mixed behavior refers to a mode where a portion of the RBCs experiences unfolding, whereas the rest of the population undergoes stretching. The percentages of stretching were (1) 27%, (2) 50%, and (3) 55%, respectively. The dashed line is a guide for the eyes representing the transition between the two modes.

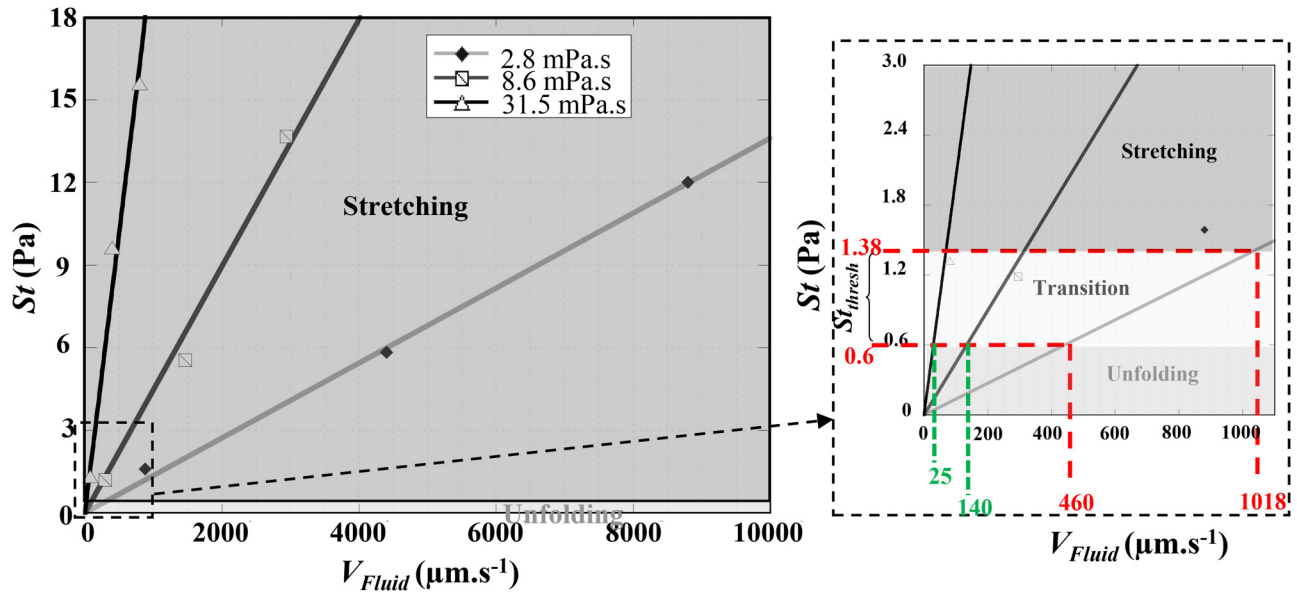

FIG. 6. Representation of the estimated applied stress St at the exit of the last geometrical constriction vs the flow velocity V_{Fluid} at this location and the external medium viscosity η_{out} showing the two behaviors regions (unfolding/stretching) as well as the threshold stress St_{thresh}. The inset shows a close-up on the origin of the plot. The gray zone represents the transition zone. Numerical simulations were performed using $W_o = 15\,\mu$m.

D. Shape recovery time

We quantified the deformation of RBCs according to the experimental conditions, i.e., at various η_{out}, V_{cell}, and for three different main channel widths ($W_o = 15$, 25, and 50 μm, all the other parameters—dimensions and number of constrictions—being maintained constant). The RBC deformation at the exit D_{out} and the associated recovery time τ_r were measured. In the case of cells returning to a steady shape according to the unfolding mode [Fig. 7(a)], the maximum deformation D_{out} experienced by cells flowing through the last geometric constriction, is independent of both parameters V_{cell} and W_o.

Indeed, in the unfolding behavior, D_{out} corresponds to the cell compression in the last narrowing, which remains constant through the whole study and, therefore, only depends on the constriction dimensions. Figure 7(b) presents the evolution of $1/\tau_r$ as a function of V_{cell}, η_{out} being fixed at 1.3 mPa s, for two values of W_o. The results show that $1/\tau_r$ is increasing linearly—thus, τ_r is decreasing—when V_{cell} increases. Such behavior has already been reported by Prado *et al.*[33] for the relaxation time measured as the time necessary for RBC, initially at rest in a capillary, to adopt a steady shape when the flow is suddenly started. We can also mention that data issued from different OWC geometries (different W_o) aligned on the same linear regression [Fig. 7(b)], hence demonstrating that the recovery time in the unfolding mode was not impacted by the width of the channel but is rather governed by the cell mechanical properties.

In the case of the stretching mode, the maximum deformation at the exit D_{out} is not influenced by the cell speed V_{cell} in the tested range (data not shown). We explain this result by the fact that although the applied stress is increased with the flow speed, RBCs transit through the high stress region more rapidly when V_{cell} increases. Consequently, the increase of St is counterbalanced by the short time RBCs spent in this region. Figure 7(c) presents the effect of W_o on D_{out}. For each external viscosity and W_o, the data from different cell speed conditions were pooled. The graph reveals that, for a fixed external viscosity ($\eta_{out} = 31.5$ mPa s), cells are more stretched at the exit of a 50 μm wide channel than when $W_o = 25$ or 15 μm. This behavior is attributed here to the fact that as St is higher than St_{thresh}, RBCs will deform according to the applied stress, which is larger in a 50 μm than in a 15 μm wide channel. In the stretching behavior, a linear relationship was retrieved between $1/\tau_r$ and V_{cell} [Fig. 7(d)]. The graph also reveals that for a given cell velocity, $1/\tau_r$ increases—i.e., τ_r decreases—when W_o is decreased, which is consistent with the fact that cells take longer time to recover from a more deformed state. Moreover, by plotting $1/\tau_r$ vs V_{cell}/W_o, we can collapse all the data on a single line as illustrated by the inset in Fig. 7(d). This indicates that, in the stretching mode, the recovery time is directly imposed by the flow. Previous studies in the literature have observed the decrease of RBC recovery time upon the increase of cell velocity and explained it through energy dissipation.[34]

We report the effect of η_{out} on RBC elongation and shape recovery at the exit. Figure 8(a) reveals that D_{out} increased as η_{out} is raised, which is consistent with the increase of the hydrodynamic stress.

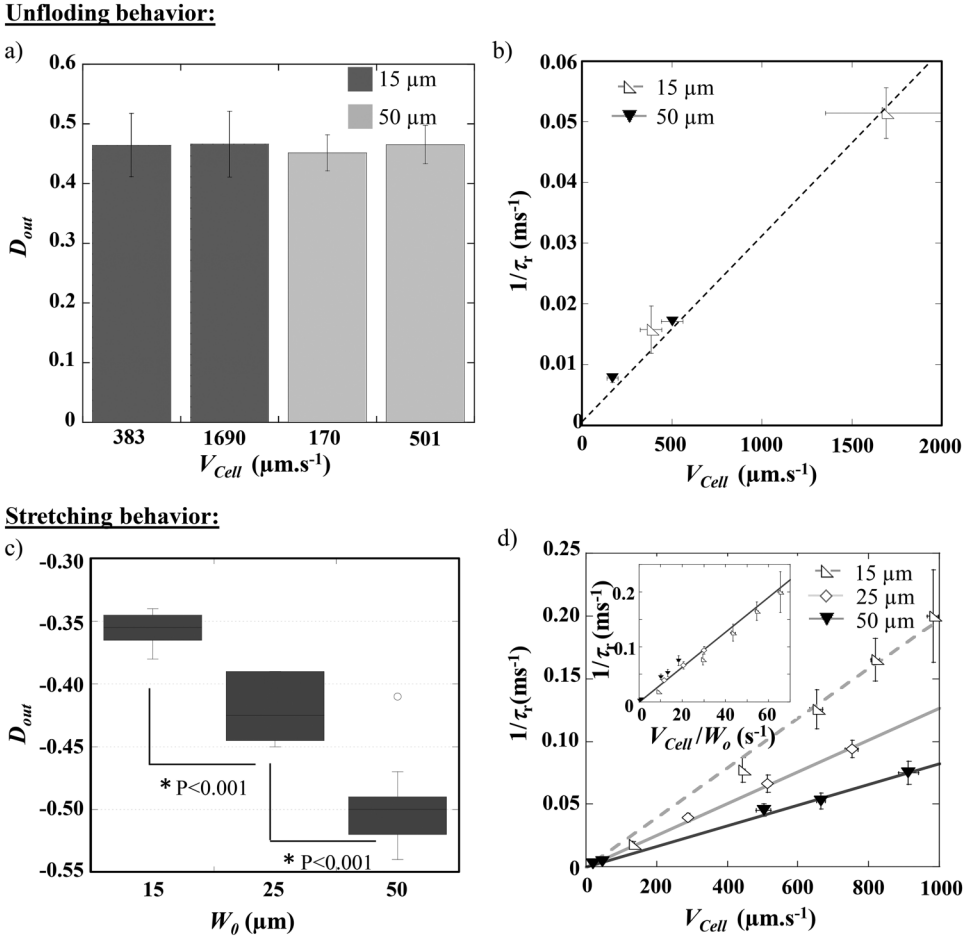

FIG. 7. Evolution of (a) the cell deformation D_{out} at the exit of the last constriction and (b) $1/\tau_r$ with the cell speed V_{cell}, for healthy RBCs experiencing the unfolding behavior in channels of different main widths W_o. The external viscosity η_{out} was set at 1.3 mPa s. (c) Evolution of D_{out} vs the main channel width W_o, for the stretching behavior ($\eta_{out} = 31.5$ mPa s). (d) $1/\tau_r$ as a function of V_{cell}, for healthy RBCs undergoing stretching at the exit of channels with different widths W_o ($\eta_{out} = 31.5$ mPa s). For both recovery modes, each point represents a statistic of at least 20 RBCs. P represents the P-value of the t-test.

One would expect to observe a longer recovery time at higher external viscosity, as more elongated cells take longer time to recover a steady shape. However, Fig. 8(b) points out that $1/\tau_r$ increases and, therefore, τ_r decreases, with the viscosity of the suspending medium. We explain this behavior in terms of a coupling between the cell and the external medium, which may impact energy dissipation. Such dependency upon η_{out} was previously observed while measuring the relaxation time using the startup flow of RBCs[33] and ecktacytometry.[34] Although such techniques report the measurement of the relaxation time, i.e., time necessary for the cells to relax to their equilibrium stress-free shape, we retrieved here the same features on the study of the time necessary to recover a steady shape while still under flow. We may notice that our measurements of τ_r in unfolding mode are starting around 129 ms, typically for $\eta_{out} = 1.3$ mPa s and $V_{cell} = 170\,\mu$m s^{-1}, which is in good agreement with relaxation time values previously reported in the literature[31,32] and predicted by the Kelvin–Voigt model. But they can also reach values as low as 4 ms, in the stretching mode for $\eta_{out} = 20.3$ mPa s and $V_{cell} = 1500\,\mu$m s^{-1}. These results illustrate that, during the flow of RBCs out of a constriction, τ_r varies with the flow conditions (i.e., η_{out} and V_{cell}/W_o). However, it can be assimilated to the cell intrinsic relaxation time dependent on the membrane mechanical properties only at very low flow speed and buffer viscosity.

E. Shape recovery time of pathological cells

Finally, we evaluated if the shape recovery time could be used to discriminate healthy from pathological RBCs. To do so, the behavior of *Plasmodium falciparum* infected RBCs (iRBCs) was studied and compared to that of healthy RBCs (hRBCs). iRBCs were obtained by culture of *Plasmodium falciparum* parasites. Parasitemia was improved by gradient centrifugation technique[21] in order to reach values of the order of 80%. iRBCs and hRBCs were flown into a 10 μm deep tooth-like microchannel—in order to avoid total blockage of the channel by pathological cells —with $W_o = 50\,\mu$m. Hydrodynamic conditions were chosen in

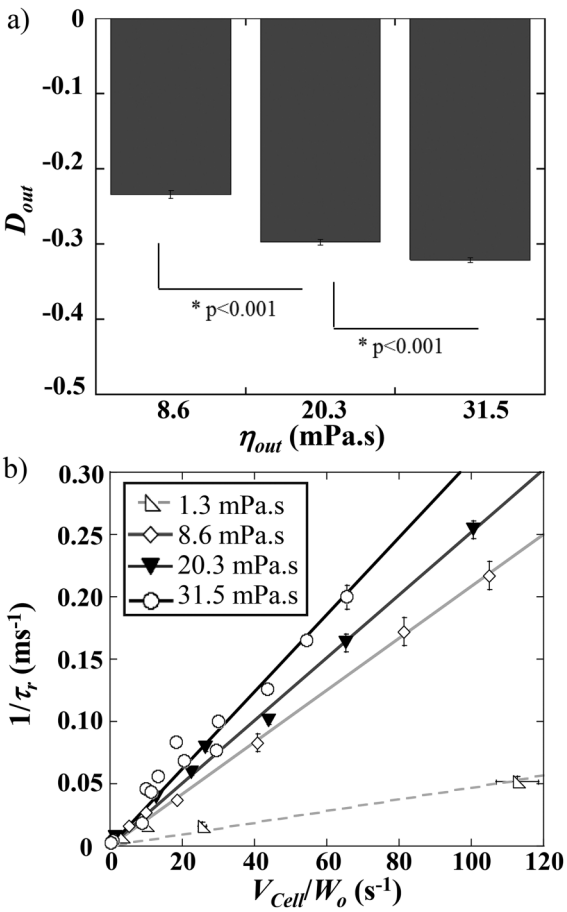

FIG. 8. (a) Evolution of D_{out} vs the external medium viscosity, η_{out}, for $W_o = 15\,\mu$m. The data have been obtained by pooling the various V_{cell} conditions for each η_{out} in the stretching mode. (b) $1/\tau_r$ as a function of V_{cell}/W_o, for various conditions of η_{out}. Each point represents a statistic of at least 20 RBCs. P represents the P-value of the t-test.

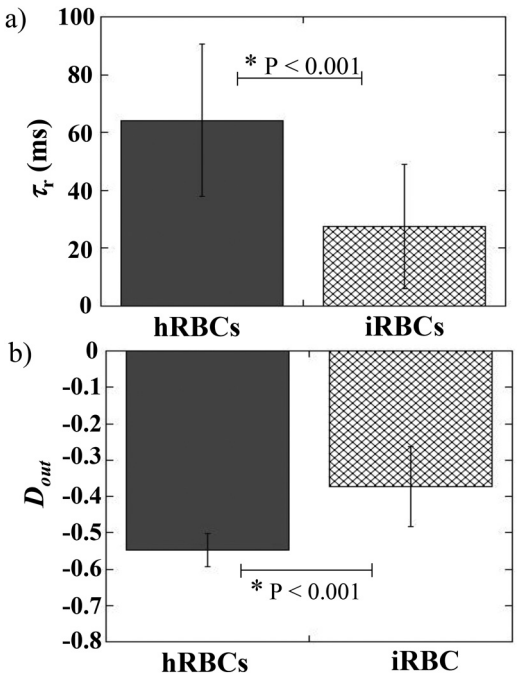

FIG. 9. (a) Shape recovery time τ_r and (b) cell elongation at the exit D_{out}, for healthy RBCs (hRBCs) and *Plasmodium falciparum* RBCs (iRBCs). P represents the P-value of the t-test calculated over roughly 50 cells for each conditions. Both populations were suspended at $\eta_{out} = 31.5$ mPa s and flown at $P = 200$ mbar in the device, leading to $V_{cell} = 1885\,\mu$m s^{-1}.

order to observe the stretching behavior, i.e., $\eta_{out} = 31.5$ mPa s and P was fixed at 200 mbar, leading to $V_{cell} \sim 1885\,\mu$m s^{-1}. The shape recovery time, τ_r, of iRBCs was estimated and compared to that of hRBCs, as presented Fig. 9(a).

The graph highlights the strong decrease in recovery time between the two samples. Indeed, iRBCs recover a stationary shape roughly twice as fast as healthy cells. This difference can be explained by the measurement of D_{out} [Fig. 9(b)], which reveals that iRBCs elongate roughly 1.6 times less than hRBCs. These findings underly that it takes less time for pathological cells to recover from a less elongated state. The measurements of shape recovery time can, therefore, be used to discriminate healthy from *Plasmodium falciparum* infected samples. Hence, demonstrating that the recovery time traduces the cell intrinsic mechanical properties, if cells undergo the same hydrodynamic stress, i.e., they are submitted to the same external viscosity and flown at the same speed, in the same geometry.

IV. CONCLUSION

Our results have shown that RBCs flowing out of a microfluidic constriction undergo two different shape recovery behaviors, depending on the experimental conditions. At high external viscosity and flow speed, we highlighted a stretching mode where the impact of the flow on the shape recovery is dominant, whereas at low viscosity and velocity of the carrier fluid, we found an unfolding mode where the mechanical phenotype of RBCs dominates the shape recovery. The calculation of the corresponding Capillary numbers shows that the RBC shear resistance governs the transition between the two recovery dynamics. It would be interesting to evaluate if the calculation of the viscous stress corresponding to the frontier between these two recovery modes (at $Ca \sim 1$) could be used to estimate an elastic shear modulus of healthy RBCs. We also showed that the associated recovery times, τ_r, vary strongly according to the viscosity and velocity of the carrier fluid. Indeed, we report values comparable with relaxation times published in the literature—and in good agreement with the Hochmuth Evans calculation based on the Kelvin–Voigt model (∼100 ms)—for very low flow speed and buffer viscosity, as well as values as low as 4 ms at specific experimental conditions. The RBCs shape the recovery under flow, being dictated by the coupling between the cell and the external medium, and it is expected that τ_r varies with the flow parameters. Indeed, we found that τ_r decreases with the raise of the

external viscosity and the relative velocity between the surrounding fluid and the RBC. We explain this reduction of the recovery time in terms of the strong coupling between the cell and the external fluid, which impacts the energy dissipation. Finally, the comparison of the behaviors of *Plasmodium falciparum* infected and healthy RBCs flowing out of constricted channels illustrates that diseased cells are less stretched and thus recover a steady shape twice as fast as normal ones. Such results demonstrate that τ_r provides a signature of the cell intrinsic mechanical properties and that its measurement has the potential to detect the pathological state of RBCs.

SUPPLEMENTARY MATERIAL

See the supplementary material for a detailed description of the preparation of the *Plasmodium falciparum* infected red blood cells. More information on the determination of cell velocity is illustrated in the supplementary material. The effect of stress history on the mechanical response of healthy RBCs is also detailed. The quantification of the centering effect of our geometry is also provided and briefly discussed. Finally, a description of the numerical simulations performed to calculate the viscous stress *St* necessary to extract the shear modulus is included.

ACKNOWLEDGMENTS

A.A. is thankful to Ecole Doctorale E.E.A. for a Ph.D. fellowship. J.E. is thankful to UCBL and INSA for postdoctoral fellowships. This work was supported by the iMUST grant. All the experiments were performed on the Nanolyon technological facilities. M.F. acknowledges the CNRS and the Mission pour les Initiatives Transverses et Interdisciplinaires for supporting the installation of an experimental setup at Institut of Parasitology and medical Mycology. The authors thank Pr. Thierry Biben for fruitfull discussions.

DATA AVAILABILITY

The data that support the findings of this study are available from the corresponding author upon reasonable request.

REFERENCES

[1]N. Mohandas and E. Evans, "Mechanical properties of the red cell membrane in relation to molecular structure and genetic defects," Annu. Rev. Biophys. Biomol. Struct. **23**, 787–818 (1994).
[2]E. A. Evans and R. M. Hochmuth, "Membrane viscoelasticity," Biophys. J. **16**, 1–11 (1976).
[3]R. M. Hochmuth, P. R. Worthy, and E. A. Evans, "Red cell extensional recovery and the determination of membrane viscosity," Biophys. J. **26**, 101–114 (1979).
[4]H. Engelhardt and E. Sackmann, "On the measurement of shear elastic moduli and viscosities of erythrocyte plasma membranes by transient deformation in high frequency electric fields," Biophys. J. **54**, 495–508 (1988).
[5]R. Waugh and R. M. Hochmuth, "Erythrocyte membrane elasticity and viscosity," Annu. Rev. Physiol. **49**, 209–219 (1987).
[6]S. Chien, K.-L. P. Song, R. Skalak, and S. Usami, "Theoretical and experimental studies on viscoelastic properties of erythrocyte membrane," Biophys. J. **24**, 463–487 (1978).
[7]R. Waugh and E. A. Evans, "Thermoelasticity of red blood cell membrane," Biophys. J. **26**, 115–131 (1979).
[8]G. B. Nash and H. J. Meiselman, "Red cell and ghost viscoelasticity. effects of haemoglobin concentration and in vivo aging," Biophys. J. **43**, 63–73 (1983).
[9]G. Tomaiuolo and S. Guido, "Start-up shape dynamics of red blood cells in microcapillary flow," Microvasc. Res. **82**, 35–41 (2011).
[10]R. M. Hochmuth, N. Mohandas, and P. L. Blackshear Jr., "Measurement of the elastic modulus for red cell membrane using a fluid mechanical technique," Biophys. J. **13**, 747–761 (1973).
[11]E. A. Evans, "Structure and deformation properties of red blood cells: Concepts and quantitative methods," Meth. Enzymol. **173**, 3–35 (1989).
[12]O. Linderkamp and H. J. Meiselman, "Geometric, osmotic, and membrane mechanical properties of density-separated human red cells," Blood **59**, 1121–1127 (1982).
[13]K. Svoboda, C. F. Schmidt, D. Branton, and S. M. Block, "Conformation and elasticity of the isolated red blood cell membrane skeleton," Biophys. J. **63**, 784–793 (1992).
[14]H. Engelhardt, H. Gaud, and E. Sackmann, "Viscoelastic properties of erythrocyte membranes in high-frequency electric fields," Nature **307**, 378–380 (1984).
[15]S. P. Sutera, R. A. Gardner, C. W. Boylan, G. L. Carroll, K. C. Chang, J. S. Marvel, C. Kilo, B. Gonen, and J. R. Williamson, "Age related changes in deformability of human erythrocytes," Blood **65**, 275–282 (1985).
[16]J. R. Williamson, R. A. Gardner, C. W. Boylan, G. L. Caroll, K. Chang, J. S. Marvel, B. Gonen, C. Kilo, R. Tran-Son-Tay, and S. P. Sutera, "Microrheologic investigation of erythrocyte deformability in diabetes mellitus," Blood **65**, 283–288 (1985).
[17]N. Mohandas, M. R. Clark, M. S. Jacobs, and S. B. Shohet, "Analysis of factors regulating erythrocyte deformability," J. Clin. Invest. **66**, 563–573 (1980).
[18]S. Braunmüller, L. Schmid, E. Sackmann, and T. Franke, "Hydrodynamic deformation reveals two coupled modes/times scales of red blood cell relaxation," Soft Matter **8**, 11240–11248 (2012).
[19]D. C. Duffy, J. C. McDonald, O. J. A. Schueller, and G. M. Whitesides, "Rapid prototyping of microfluidic systems in poly(dimethylsiloxane)," Anal. Chem. **70**, 4974–4984 (2004).
[20]W. Trager and J. B. Jensen, "Human malaria parasites in continuous culture," Science **193**, 673–675 (1976).
[21]S. Kutner, W. V. Breuer, H. Ginsburg, S. B. Aley, and Z. I. Cabantchik, "Characterization of permeation pathways in the plasma membrane of human erythrocytes infected with early stages of plasmodium falciparum: Association with parasite development," J. Cell. Physiol. **125**, 521–527 (1985).
[22]G. Blankenstein and U. Larsen, "Modular concept of a laboratory on a chip for chemical and biochemical analysis," Biosens. Bioelectron. **13**, 427–438 (1998).
[23]L. Rico, J. Juncá, M. Ward, J. Bradford, J. Bardina, and J. Petriz, "Acoustophoretic orientation of red blood cells for diagnosis of red cell health and pathology," Sci. Rep. **8**, 15705 (2018).
[24]D. Schrum, C. Culbertson, S. Jacobson, and J. Ramsey, "Microchip flow cytometry using electrokinetic focusing," Anal. Chem. **71**, 4173–4177 (1999).
[25]Y. Kim and J. Yoo, "Three-dimensional focusing of red blood cells in microchannel flows for bio-sensing applications," Biosens. Bioelectron. **24**, 3677–3682 (2009).
[26]M. Faivre, M. Abkarian, K. Bickraj, and H. A. Stone, "Geometrical focusing of cells in a microfluidic device: An approach to separate blood plasma," Biorheology **43**, 147–159 (2006).
[27]A. Abay, S. Recktenwald, T. John, L. Kaestner, and C. Wagne, "Cross-sectional focusing of red blood cells in a constricted microfluidic channel," Soft Matter **16**, 534–543 (2020).
[28]C. Tsai, S. Sakuma, F. Arai, T. Taniguchi, T. Ohtani, Y. Sakata, and M. Kaneko, "Geometrical alignment for improving cell evaluation in a microchannel with application on multiple myeloma red blood cells," RSC Adv. **4**, 45050–45058 (2014).
[29]G. Tomaiuolo, M. Barra, V. Preziosi, A. Cassinese, B. Rotoli, and S. Guido, "Microfluidics analysis of red blood cell membrane viscosity," Lab Chip **11**, 449–454 (2011).
[30]E. A. Evans, "Bending elastic modulus of red blood cell membrane derived from buckling instability in micropipette aspiration tests," Biophys. J. **43**, 27–30 (1983).

[31]E. A. Evans, "New membrane concept applied to the analysis of fluid shear- and micropipette-deformed red blood cells," Biophys. J. **13**(9), 941–954 (1973).
[32]S. Hénon, G. Lenormand, A. Richert, and F. Gallet, "A new determination of the shear modulus of the human erythrocyte membrane using optical tweezers," Biophys. J. **76**, 1145–1151 (1999).
[33]G. Prado, A. Farutin, C. Misbah, and L. Bureau, "Viscoelastic transient of confined red blood cells," Biophys. J. **108**, 2126–2136 (2015).
[34]O. K. Baskurt and H. J. Meiselman, "Determination of red blood cell shape recovery time constant in a couette system by the analysis of light reflectance and ektacytometry," Biorheology **33**, 489–503 (1996).